ADVANCING EARTH AND SPACE SCIENCES

JGR Space Physics

RESEARCH ARTICLE
10.1029/2024JA033349

Special Collection:
Recent Advances on Modelling and Observations in Space and Earth Sciences

Key Points:

- A train of patches exhibits the "wave-like" evolution associated with the magnetopause reconnection and magnetotail reconnection
- The duskward tilted convection pattern, impacted by IMF By, partially contributes to patch spatial spread toward the nightside sector
- This work provides the evidence for extended magnetic reconnection in the dusk magnetotail

Supporting Information:
Supporting Information may be found in the online version of this article.

Correspondence to:
Q.-H. Zhang,
zhangqinghe@nssc.ac.cn

Citation:
Zhang, D., Zhang, Q.-H., Oksavik, K., Tang, B.-B., Zhang, Y.-L., Lockwood, M., et al. (2024). A "wave-like" evolution of polar cap patches modulated by enhanced magnetopause reconnection and extended magnetotail reconnection. *Journal of Geophysical Research: Space Physics*, *129*, e2024JA033349. https://doi.org/10.1029/2024JA033349

Received 19 SEP 2024
Accepted 14 DEC 2024

A "Wave-Like" Evolution of Polar Cap Patches Modulated by Enhanced Magnetopause Reconnection and Extended Magnetotail Reconnection

Duan Zhang[1], Q.-H. Zhang[1,2], K. Oksavik[3,4], B.-B. Tang[1], Y.-L. Zhang[5], M. Lockwood[6], J. C. Foster[7], S.-R. Zhang[7], Larry R. Lyons[8], Z.-Y. Xing[2], Yong Wang[2], and Y.-Z. Ma[2]

[1]State Key Laboratory of Space Weather, National Space Science Center, Chinese Academy of Sciences, Beijing, China, [2]Shandong Provincial Key Laboratory of Optical Astronomy and Solar-Terrestrial Environment, Institute of Space Sciences, Shandong University, Weihai, China, [3]Department of Physics and Technology, University of Bergen, Bergen, Norway, [4]Arctic Geophysics, University Centre in Svalbard, Longyearbyen, Norway, [5]The Johns Hopkins University Applied Physics Laboratory, Laurel, MD, USA, [6]Department of Meteorology, University of Reading, Earley Gate, UK, [7]MIT Haystack Observatory, Westford, MA, USA, [8]Department of Atmospheric and Oceanic Sciences, University of California, Los Angeles, CA, USA

Abstract A train of large-scale polar cap patches was observed in the ionosphere during a period of southward interplanetary magnetic field (IMF) during the main phase of a moderate geomagnetic storm. The patches were sequentially detached from a dayside storm enhanced density plume through cusp dynamics due to pulsed enhancement of the dayside magnetic reconnection rate, suggested by the increase of the Kan-Lee electric field and cross polar cap potential. After formation and IMF By duskward turning, the patches propagated obliquely like "waves" in the polar cap toward the dusk sector, and exited the polar cap over a wide magnetic local time (MLT) region (18–24 MLT). Simulations under a strongly southward IMF Bz and duskward IMF By show that the magnetotail magnetic reconnection occurs over a broad MLT range. Such a tail reconnection modulates the evolution of the patches.

1. Introduction

Polar cap patches are the high-density plasma structures in the polar ionosphere with the spatial size of hundreds to thousands of kilometers (Crowley, 1996; Zhang et al., 2020). Ionospheric uplift by prompt penetration electric fields (PPE) during a geomagnetic storm leads to a large-scale electron density enhancement occurs in the mid-latitude ionosphere produced by solar extreme ultraviolet (EUV) radiation ionization. Driven by sub-auroral polarization stream (SAPS) electric fields (Foster & Burke, 2002), plumes of storm enhanced density (SED) (Foster, 1993; Foster et al., 2021) are conveyed to high latitudes in the noon sector where they can serve as a source plasma for the polar cap patches or the tongue of ionization (TOI) through magnetosphere-ionosphere-thermosphere (M-I-T) coupling process (such as variable ionospheric convection and the dayside open-closed field line boundary (OCB) variations associated with the magnetopause reconnection) (Foster et al., 2005; Knudsen, 1974; Lockwood et al., 2005; Oksavik et al., 2006; Zhang, Zhang, Hu, et al., 2013).

After their formation, the polar cap patches often move along the streamlines of the polar ionospheric convection pattern from the dayside to the nightside under the effect of the convection electric field (Zhang, Zhang, Lockwood, et al., 2013, 2015, 2016, 2020; Oksavik et al., 2010), and then cross the nightside polar cap boundary (PCB) leaving the polar cap driven by the nightside magnetotail reconnection (Moen et al., 2007, 2008; Wood et al., 2009), which is the only way for the polar cap patches to leave the polar cap (Lorentzen et al., 2004). During this evolution process, the changing ionospheric convection pattern represents the variation of the Earth's magnetic field configuration, which is modulated by the solar wind and interplanetary magnetic field (IMF) (Cowley, 1982; Pettigrew et al., 2010; Ruohoniemi et al., 2002). For example, when the IMF By is positive (negative) in the Northern (Southern) Hemisphere, the duskside cell becomes rounder and the dawnside cell becomes narrower like a banana (Grocott et al., 2010; Hairston & Heelis, 1995), which may affect the dawn-dusk drift of the polar cap patches. Moreover, when the IMF Bz is positive (northward), the high-latitude lobe magnetic reconnection can occur (Lockwood & Moen, 1999), resulting in a reverse convection cell, which may accelerate or decelerate the movement of the polar cap patches (Hosokawa et al., 2011; Oksavik et al., 2010). Therefore, the dayside magnetopause reconnection, nightside magnetotail reconnection, and ionospheric convection are very important for the formation and evolution of the polar cap patches.

Various instruments can be used to investigate the formation and evolution of polar cap patches. For example, Zhang, Zhang, Lockwood, et al. (2013) used total electron content (TEC) from GPS receivers (Coster et al., 2003) and the large-scale convection flows provided by the SuperDARN radars (Chisham et al., 2007) in the polar region to directly observe the patch evolution relative to polar convection. Lorentzen et al. (2010) used high-resolution all-sky imager and European Incoherent Scatter Svalbard Radar data to present a model that patches can be induced by a poleward moving auroral form (PMAF). Moreover, there are some studies using in-situ data to analyze the key plasma parameters of patches. For example, Ma et al. (2018) used the thermal plasma analysis package of Special Sensors-Ions, Electrons, and Scintillation (SSIES) and Special Sensor for Precipitating Particles (SSJ/5) on board the Defense Meteorological Satellite Program (DMSP) satellites (Greenspan et al., 1986; Hardy et al., 2008) to characterize the field-aligned current (FAC) and particle precipitation associated with the polar cap patches. These instruments offer detailed information for analyzing the characteristics of patch evolution from different aspects.

Thus, in this paper, we combine space-based and ground-based observation data to investigate the effects of dayside magnetopause reconnection and extended nightside magnetotail reconnection on the morphology and motion of the polar cap patches, and we explain the modulating role of IMF and the magnetotail reconnection on polar cap patch evolution.

2. Observations and Results

2.1. Solar Wind, IMF, and Geomagnetic Conditions

On 27 February 2014, a moderate geomagnetic storm occurred due to the impact of a shock in solar wind on the magnetopause at about 17:00 UT. The solar wind, IMF and geomagnetic conditions are presented in Figure 1. Parameters in Figure 1 are: (a) three IMF components in Geocentric Solar Magnetic (GSM) coordinates, (b) the solar wind number density and velocity, (c) the solar wind dynamic pressure, P_{Dyn}, and the SYM-H index, (d) the cross polar cap potential (CPCP, associated with the solar wind coupling process (Mori & Koustov, 2013)), (e) the auroral electrojet (AE) indices (AE = AU-AL). The IMF and solar wind data have been lagged by 42.9 min to allow the data to propagate from the satellite to the ionosphere by fitting the shock arrival and storm onset identified from the SYM-H index. Before the shock impact (~16:50 UT, marked by the black vertical dashed-line in Figure 1), the IMF and solar wind conditions were weak and stable (Figures 1a–1c), leading to quiet geomagnetic conditions and small CPCP (Figures 1c–1e). After about 16:50 UT, however, the IMF and solar wind had strong variations (Figures 1a–1c), resulting in a moderate geomagnetic storm, strongly varying CPCP, a series of substorms (Figures 1d and 1e). The gray area between the two red vertical dashed-lines highlights the interval of interest. The IMF Bz component was mainly negative around −10 nT with four positive excursions around 18:10 UT, 19:30 UT, 20:10 UT and 21:56 UT, the IMF By component was negative before 18:50 UT and after 21:57 UT and stayed positive (duskward) between them, and Bx varied around zero (see Figure 1a); while the solar wind was stable at high speed (~460 km/s) and number density (~18 cm^{-3}), giving a high dynamic pressure (~7 nPa). These IMF conditions are favorable for reconnection at the dayside magnetopause (Koga et al., 2019; Scurry et al., 1994). This interval was the period of the main phase of the storm with four CPCP enhancements and substorms at the beginning and end (Figures 1c–1e).

2.2. GPS TEC Data and SuperDARN Convection Maps

Figure 2 shows the formation and evolution of patches, as revealed by mapping of the GPS TEC and the SuperDARN convection patterns. The TEC data from the Madrigal database has a time resolution of 5 min and a spatial resolution of 1° × 1° in geographic latitude and geographic longitude, which were transferred into the altitude-adjusted corrected geomagnetic (AACGM) coordinates and median-filtered for smoothening. The white area represents TEC data gaps. The SuperDARN convection patterns were obtained by using the RG96 model with "Map Potential" technique (Ruohoniemi & Baker, 1998; Thomas et al., 2013), based on the actual radar line-of-sight velocities. The black thick curves/ellipses mark the TEC SED, TOI and polar cap patches, the evolution of which are followed here. The SuperDARN convection patterns from the Virginia Tech SuperDARN website have a time resolution of 2 min and a spatial resolution of 1° × 1° in AACGM magnetic latitude (MLAT)/MLT coordinates. For better comparison with the 5-min averaged TEC data, we only selected the convection data in the

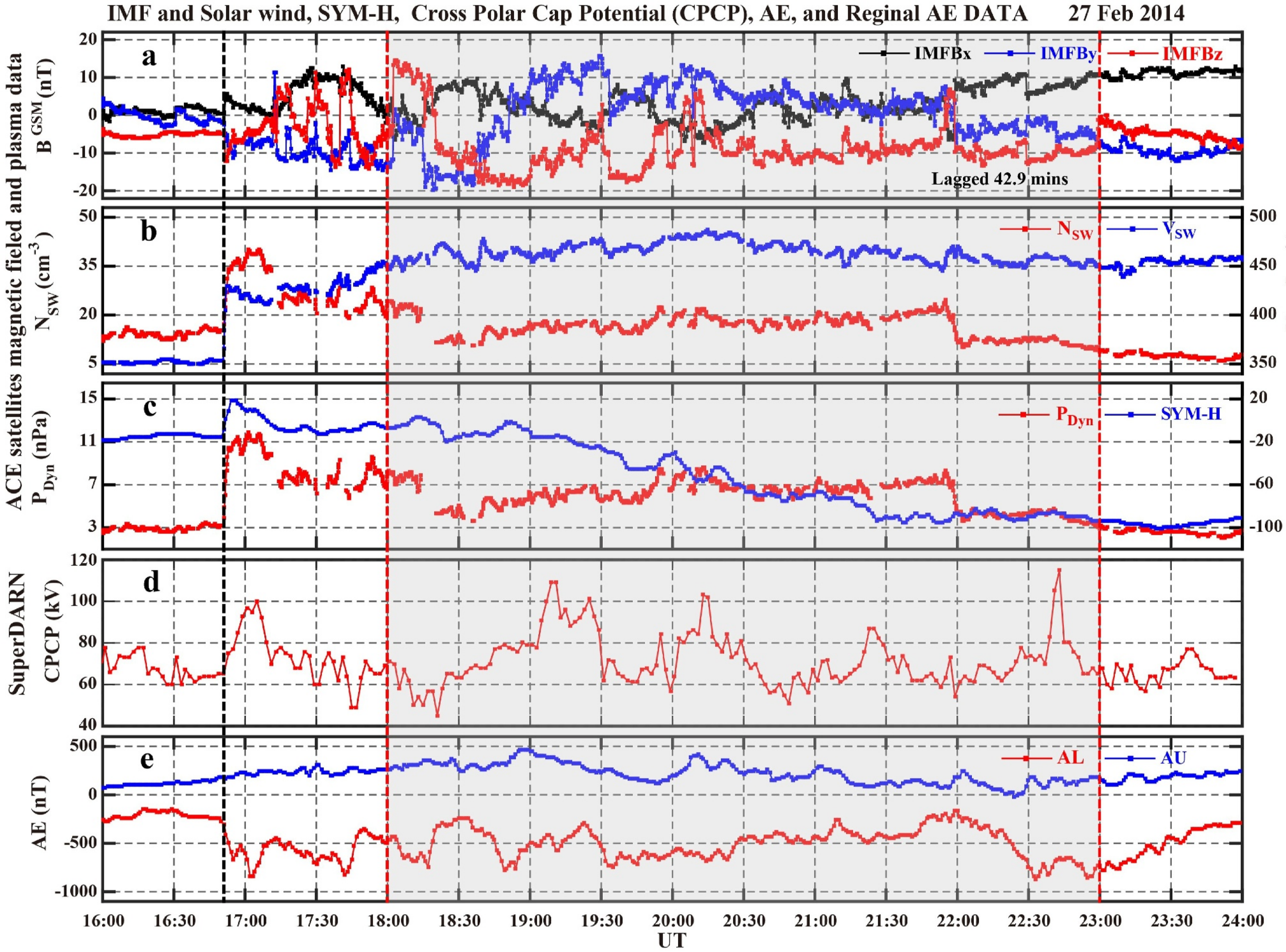

Figure 1. An overview of the solar wind and IMF conditions observed by the ACE satellite, together with the geomagnetic indices (SYM-H and AE indices). Parameters shown are: (a) the GSM IMF components, (b) the solar wind plasma number density and speed, NSW and VSW; (c) the solar wind dynamic pressure, PDyn, and the SYM-H index; (d) the SuperDARN cross polar cap potential (CPCP), (e) the auroral electrojets (AE) index, AU and AL. The IMF and solar wind data have been lagged by 42.9 min to allow the data to propagate from the satellite to the ionosphere by fitting the shock arrival and storm onset. The SMU and SML indices are derived from the magnetometer data provided by the SuperMAG collaborators and are the upper and lower envelopes of the N-component for stations between 40° and 80° magnetic north, respectively.

middle of every 5-min interval, for example, the convection data between 19:22 and 19:24 UT for comparison with the TEC data between 19:20 and 19:25 UT. The colored thick line in Figure 2f represents the O^+ number density (data shown in Figure 3) along the projected orbit trace of DMSP F17 from 20:58 to 21:22 UT with black dots marking the time ticks.

Figure 2a shows large values of GPS TEC in the dayside lower latitude region due to the solar EUV ionization and a typical two-cell convection pattern as observed by SuperDARN radars. The region of high-density sunlit plasma is slightly inclined toward the dusk sector. An old polar cap patch appeared in the TEC data at the nightside of the magnetic north pole, where the TEC was generally small including most part of the convection pattern and the lower latitude region of the nightside sector. This patch was formed earlier at about 17 UT in the dayside cusp region and traversed across the north pole to the midnight sector along the convection streamlines. Compared with Figure 2a, the two-cell convection pattern consequentially expanded equatorward resulting in an increase of CPCP to reach a peak of about 110 kV at about 19:10 UT (Movie S1, Figures 1d and 2b). This is the expected response to a period of strong southward IMF conditions (Siscoe, 1982), and it drove the high-density plasma (high TEC) at the low-latitude afternoon sector toward the high-latitude noon sector to form a large-scale SED plume and to enter the polar cap forming a TOI (Figure 2b). After this expansion, the CPCP started to decrease and reached a valley at about 19:40 and 19:50 UT, suggesting the polar cap boundary (PCB) contracted poleward

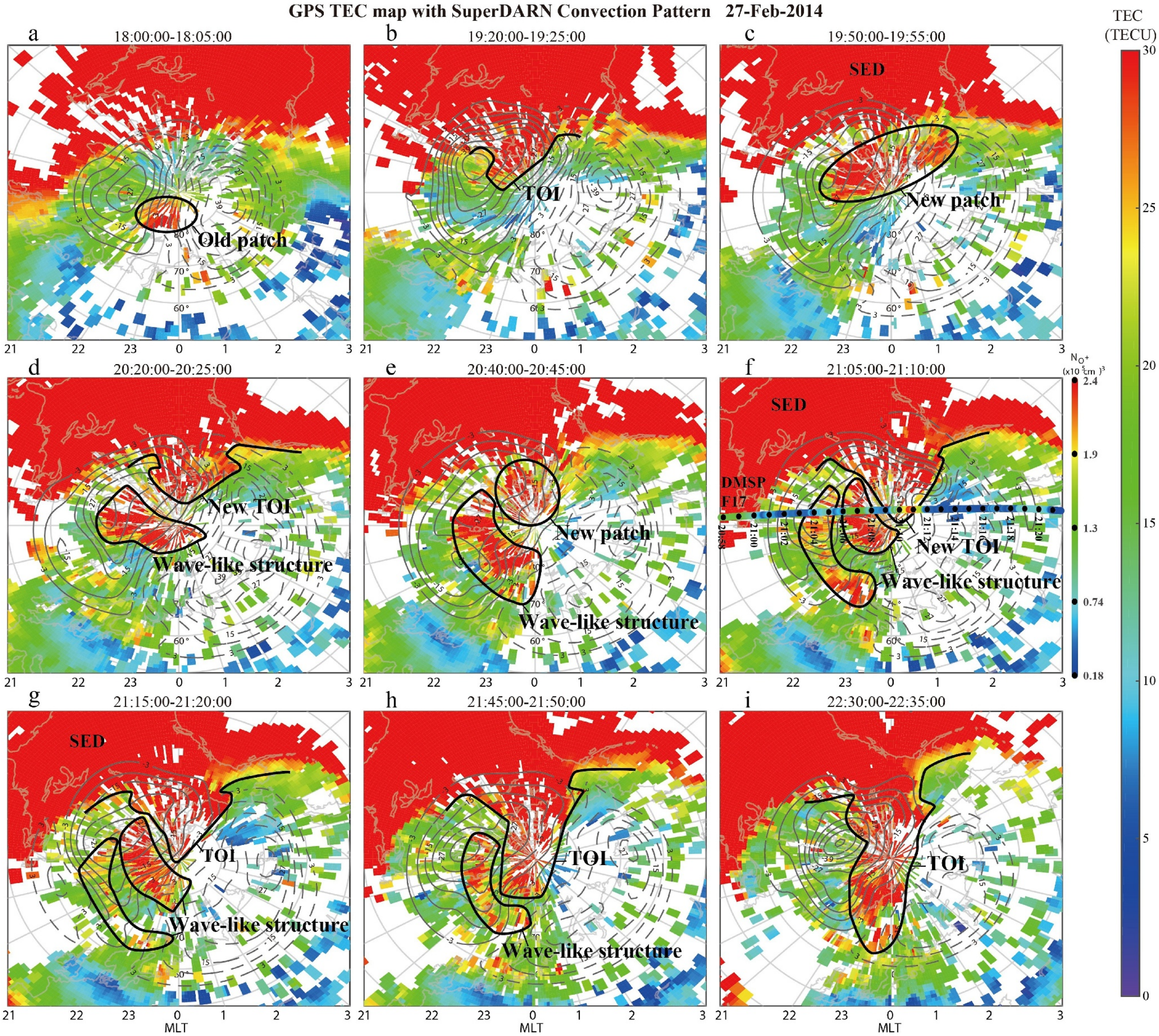

Figure 2. Selected examples from a full series of 2-D maps of median-filtered TEC and ionospheric convection on a geomagnetic latitude/MLT grid with noon at the top. The black thick curves/ellipses mark the TEC SED, TOI and polar cap patches, the evolution of which are followed here. The colored thick line in (f) represents the O^+ number density (data from which are shown in Figure 3) along the projected orbit trace of DMSP F17 from 20:58 to 21:22 UT with black dots marking the time ticks.

and detached the dayside SED plume (or TOI) into a large-scale plasma patch (Figure 2c) (Carlson et al., 2004; Lockwood & Carlson, 1992). The strengthening and weakening of the CPCP index made the high- and low-density plasma alternately enter the polar cap, forming the initial "wave-like" structure.

The first new patch was elongated in the northeast direction right after its formation (Figure 2c); however, it changed its shape in "wave-like" structure and twisted in the northwest direction with decaying of its density during its transpolar evolution (Figures 2d and 2e). During the evolution, this patch was almost completely in the dusk convection cell and it was the distortion of the convection pattern caused by the IMF By turning from negative to positive that gave the patch its evolving shape. When the patch arrived at the duskside and nightside PCB, it exited the polar cap over a wide region (18–24 MLT), after which it broke into multiple "blobs" and further decayed to almost disappear in the auroral sunward return flow region in the dusk to midnight sector (Figures 2f–2h). During the evolution of the first patch, a new TOI formed when the CPCP reached a new peak of about 102 kV around 20:20 UT (Figures 1e and 2d). A second large-scale patch detached from the new TOI when

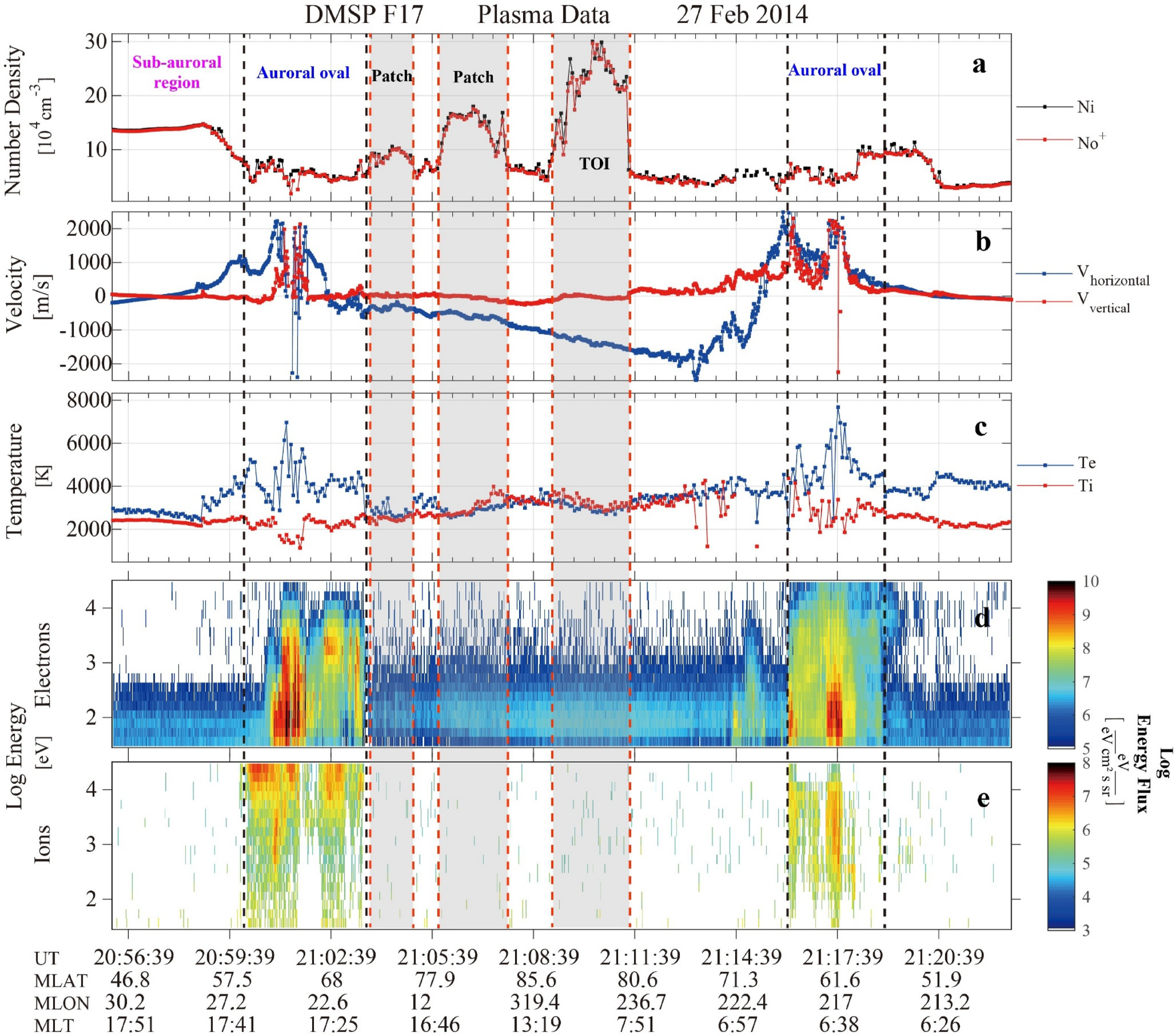

Figure 3. In-situ plasma parameters measured by DMSP F17. Parameters shown are: (a) plasma number densities for O^+ and total ions, (b) the cross-track horizontal and vertical ion flows, (c) the ion and electron temperature, (d) the electron energy flux, and (e) the ion energy flux. The vertical dashed lines separate the approximate locations of the auroral zone and polar cap patches and TOI (also highlighted by the gray area), respectively.

the CPCP decreased to a new valley (Figures 1e and 2e). The second patch had almost the same behavior as the first patch, due to the similar interplanetary condition (strong southward IMF with positive By components and stable solar wind parameters, Figures 1a–1c) and geomagnetic conditions (main phase of the storm within a sequential substorm, Figures 1c and 1d).

During the interval of interest, a third TOI formed around 21:00 UT, and the CPCP increased correspondingly with the peak value of 87 kV at 21:26 UT. However, this TOI was not clearly detached into patches (or unable to distinguish due to the spatial resolution limitation of the TEC data) and almost straightly propagated to the midnight sector until the end of the interval of interest. The persistence of this TOI may have resulted from the steadiness of the IMF after its formation, and the straight propagation across the polar cap, rather the curvature toward the duskside, may have resulted from the weakening IMF By.

In Figures 2f and 2g, the "wave-like" structure and the third TOI coexisted in the polar cap region, which was confirmed by the well-defined enhancements in the O^+ number density when the DMSP F17 satellite traversed

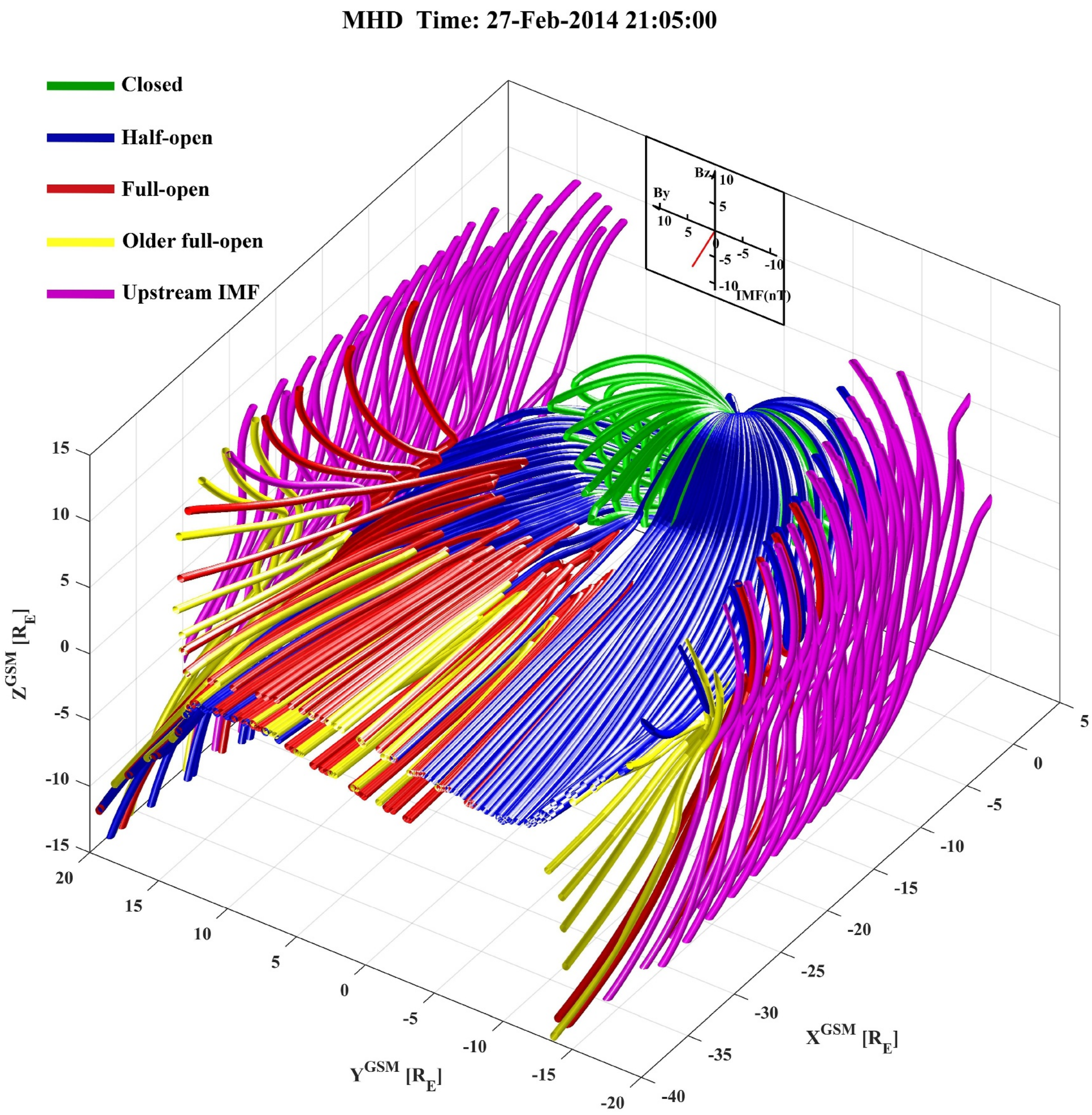

Figure 4. A 3-D view of the selected magnetic field lines simulated by the PPMLR-MHD code at 21:05 UT on 27 February 2014. The green lines represent closed field lines with two ends linked to the Earth. The blue lines are half-open field lines with one end linked to the Earth and the other end linked to the IMF. The red lines are in the magnetotail as newly full-open field lines generated by tail reconnections. The yellow lines are in the magnetotail as older full-open field lines generated by tail reconnections. They are anti-sunward from the tail reconnection region. The pink lines represent the upstream IMF, where the IMF vector is highlighted in the coordinate system in the mid-upper box in the Y-Z plane at $X = 5$ R_E.

them (Figure 2f). These satellite observations are shown in Figure 3. DMSP F17 crossed the evening (17 MLT) SAPS flow channel between 20:58 and 21:00 UT (Figure 3b) where the sunward ion velocity reached 1,000 m/s. At the satellite altitude, the density was 10^5 cm^{-3}, yielding a 10^{14} m^{-1}s^{-1} sunward ions flux. At the subsatellite point, vertical TEC was about 35 TECu (1 TECu represents an integrated column density of 10^{16} electrons m^{-2}). A 1,000 m/s SAPS flow over 3 deg of latitude would transport $\sim 10^{26}$ ions/sec in the SED plume toward the noontime cusp. In similar circumstances, Foster et al. (2004) reported sunward fluxes of 10^{26} - 10^{27} ions/sec in the SED plume (Goldstein & Sandel, 2005). In the auroral zone, the plasma number density was not consistently enhanced in the topside ionosphere (about 860 km, Figure 3a), with only a weak enhancement seen in the dawn oval later in the pass (Figure 3a); the ion velocity was mainly sunward and upward with flow shears (Figure 3b); the electron temperature was largely enhanced but the ion temperature shows some decrease (Figure 3c); the energy fluxes showed strong particle precipitation both for elections and ions (Figures 3d and 3e).

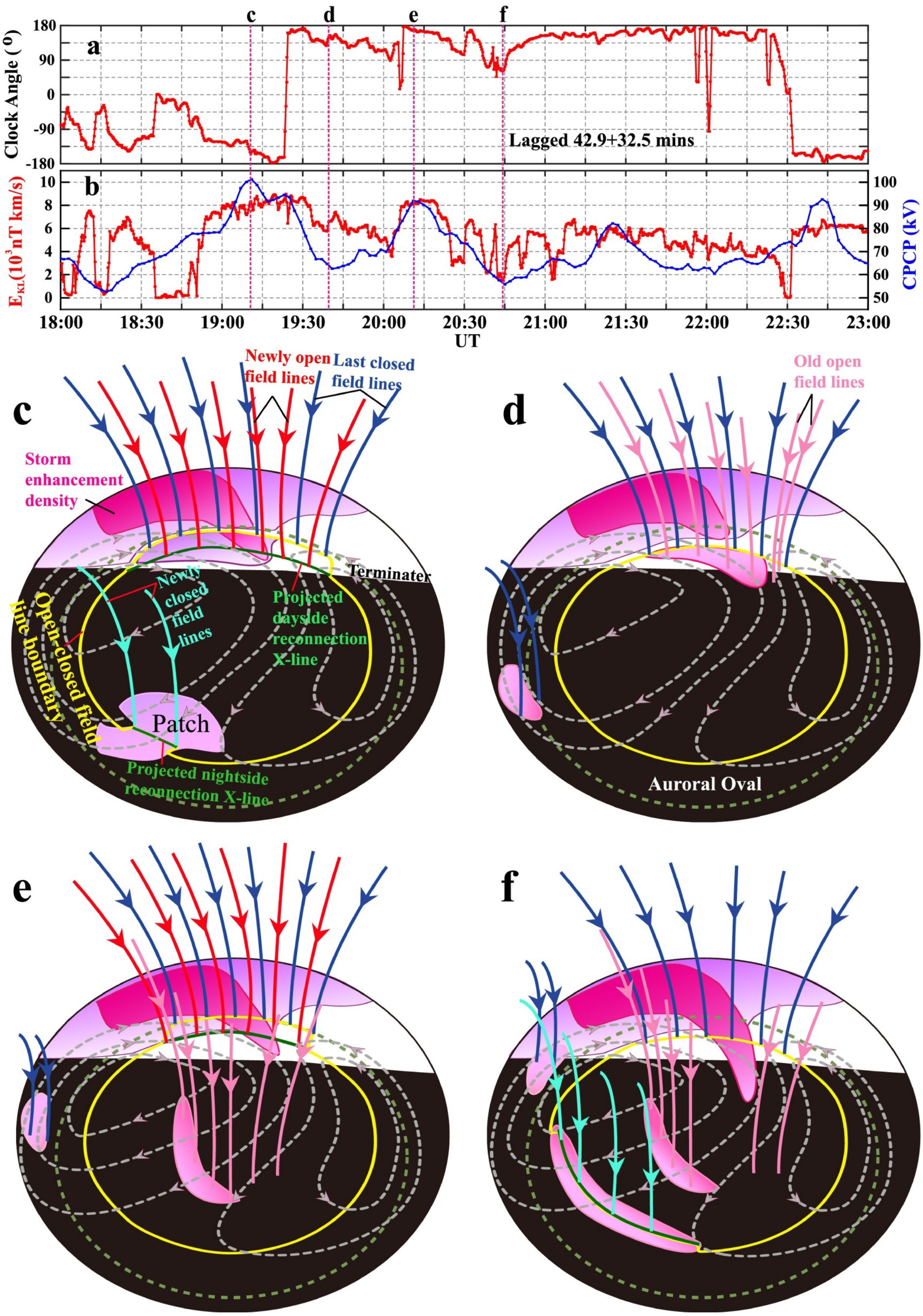
c
d
e
f
180
90
0
-90
-180
Clock Angle (°)
a
Lagged 42.9+32.5 mins
b
10
8
6
4
2
0
$E_{KL}(10^3 nT km/s)$
100
90
80
70
60
50
CPCP (kV)
18:00
18:30
19:00
19:30
20:00
20:30
21:00
21:30
22:00
22:30
23:00
UT
Newly open field lines
Last closed field lines
Storm enhancement density
Terminater
Newly closed field lines
Projected dayside reconnection X-line
Open-closed field line boundary
Patch
Projected nightside reconnection X-line
Old open field lines
Auroral Oval

Figure 5.

After entering the polar cap, the satellite measured three separate structures of enhanced ion density which match the two patches and one TOI in the TEC map in Figure 2f. Inside these structures, the electron temperature was similar with ion temperature, and the precipitation was polar rain (Zhang et al., 2007). There was a substantial increase in the anti-sunward flow as the DMSP F17 moved from dusk to dawn, which is consistent with the SuperDARN convection patterns and reflects the positive IMF By. Note that the ion density in these three structures gradually increased as the satellite entered deeper into the polar cap, which was consistent with the decay of the patches seen in the TEC maps. Outside of these structures, the satellite measured roughly stable conditions in all parameters, except for the strong varied horizontal velocities and strong precipitation in the dawnside polar cap.

3. Discussion

In Figure 2c, SED was the high-density plasma source, and formed the patches in the cusp under the effect of cusp dynamics. The patch was elongated in the northeast direction firstly. When IMF By turned positive (duskward), it was twisted to stretch in the northwest direction and evolved toward the pre-midnight sector. Then, there were two more new additional patch/TOI that formed and evolved following the first patch across the polar cap as a "wave-like" structure. Finally, these patches arrived at the nightside polar cap boundary (PCB), and exited the polar cap over very wide areas (about 18–24 MLT). This indicates ongoing magnetotail reconnection across wide MLT regions, because transport across the nightside polar cap boundary requires ongoing magnetotail reconnection (Zhang, Zhang, Hu, et al., 2013, 2015). Moen et al. (2007) provided statistics showing that patches exit the polar cap from ∼18:30 and 05:30 MLT with most patches exiting within a ∼3–4 hr wide region centered on 23:30 MLT. For a patch to exit the polar cap, however, ongoing magnetotail reconnection is required necessarily. Without this process, the polar cap boundary is "adiaroic" (see Figure 5) and the patch can only migrate slowly equatorward with the expanding polar cap boundary (see in Figures 2d–2h) and would remain confined within the nightside polar cap. Here, the "wave-like" structure refers to how multiple patches are arranged from the dayside to the nightside, gradually lengthening along the zonal direction, and their boundary curvatures all point toward the same center. It is also worth noting that some small-scale structures seem to exist along the patch. Hosokawa et al. (2013, 2016) found similar small-scale structures at the trailing edge of the patch using all-Sky Imager observations, and suggested that these structures were related to gradient-drift instability (GDI).

To investigate whether the ongoing magnetotail reconnection occurred across wide MLT regions or not, we ran a high-resolution 3-D global magnetohydrodynamics (MHD) code driven by the observed solar wind and IMF parameters. The MHD code uses piecewise parabolic method (Colella & Woodward, 1984) with a Lagrangian remap to MHD (PPMLR-MHD) imbedded in an electrostatic ionosphere shell with height-integrated conductance allowing for the electrostatic coupling and calculation of FACs between the ionosphere (near the Earth) and the model's magnetospheric inner boundary (about 3 R_E) (Hu et al., 2007; Tang & Wang, 2018). Figure 4 shows one snapshot of the simulation results: the 3D topology of selected magnetic field lines in the magnetotail and both flanks. Figure 4 reveals that the ongoing magnetotail reconnection occurred across a wide region, from midnight (around 24 MLT) to the dusk flank (around 18 MLT), which is characterized by the folded red and yellow full-open field lines. This suggests that the polar cap patches could be widely stretched near the exit, which is indeed related to the extended ongoing magnetotail reconnection. The geomagnetic activity level, solar wind energy input, and IMF Bz are likely to stimulate the extended magnetotail reconnection. The magnetotail reconnection

Figure 5. Schematic representation of the formation and evolution of polar cap patches in the Northern Hemisphere when IMF turned from southwest to southeast. Panels shown are: (a) the IMF clock angle observed by the ACE satellite, (b) the Kan-Lee electric field calculated from the ACE magnetic field and plasma observations overlaid the SuperDARN cross polar cap potential (CPCP), and (c)–(f) the formation and evolution of patches in the polar ionosphere. The ACE data has been shifted by 42.9 min to account for the solar wind propagation from the satellite to the ionosphere and by 32.5 min for better match with the ionospheric convection response (represented by CPCP) to enhanced Kan-Lee electric field. The magenta vertical dashed lines in (a) and (b) mark the interplanetary conditions of the ionosphere for panels (c)–(f), respectively. The convection streamlines in panels (c)–(f) are in dashed gray. The boundary between open and closed field lines (OCB) lies close to the poleward edge of the auroral oval. The green OCB segments with blue/cyan vertical field lines show where magnetic reconnection at the magnetopause/magnetotail is generating/destroying open flux in the Dungey convection cycle (Dungey, 1961; Zhang, Zhang, Lockwood, et al., 2013, 2015). The yellow OCB segments are "adiaroic" (meaning "not flowing across") where flow streamlines cross the OCB because it is in motion and the plasma moves with it. The magenta vertical field lines represent the open-flux polar cap, and the blue vertical lines represent the closed field line region. The color-coded areas indicate high plasma concentration. The lilac-white shading represents the underlying photo-ionized plasma at lower latitudes, within which the pink-gray shading represents the denser plasma of SED (or TOI) transported from mid-latitude. The pink-gray shadings represent the detached patches.

sites usually have a higher occurrence on the duskside centered at Y_{GSM}≈4–8 R_E (corresponding ~22–23 MLT) (Nagai et al., 2023). When geomagnetic activity and solar wind energy input increases, the magnetotail reconnection sites may expand to both the dawnside and the far-duskside (Genestreti, 2016). Moreover, the continuous southward IMF Bz and substorm activity tend to shift the magnetotail reconnection sites further duskward (Nagai et al., 2023). This result also indicates that the spatial distribution of magnetotail reconnection may be more extensive than previously recognized, which has important implications for understanding the magnetosphere-ionosphere coupling process.

Figures 5c–5f schematically illustrate the evolution of the "wave-like" structure. Figures 5a and 5b show the IMF clock angle (θ = atan (By/Bz)) and E_{KL} (roughly representing the dayside reconnection rate). The IMF data has been shifted by 42.9 min to account for the solar wind propagation from the satellite to the ionosphere and by 32.5 min to allow for a better fitting of the ionospheric convection response (represented by CPCP) to the enhanced E_{KL}. Due to the IMF By turning positive (duskward), the IMF clock angle turned from about −180° to 180° around 19:20 UT and from 180° back to −180° around 22:30 UT. The IMF By component can be introduced into the magnetotail on a timescale of approximately 25 min through the magnetospheric propagation of a compressional MHD wave formed by the perturbation due to dayside reconnection (Tenfjord et al., 2015). The E_{KL} showed two big enhancements between about 18:40 and 20:40 UT, suggesting increased reconnection rate, expansions of the convection pattern (enhanced CPCP), and formation of polar cap patches (Lockwood & Carlson, 1992). After the IMF duskward turning, the ionospheric convection pattern is partly titled duskward, and the polar cap patches are twisted accordingly. When these patches reached the polar cap boundary, they were further stretched along the zonal direction due to the extended magnetotail reconnection. Thus, combining the above effects, the patches propagated obliquely like "waves" in the polar cap toward the dusk sector and exited the polar cap at about 70° MLAT through a wide region along the zonal direction (18–24 MLT). This unusual evolution took about 2–3 hr, which is consistent with the predictions from the previous theories, observations and trajectory analysis techniques. For example, using the trajectory analysis technique, Zhang et al. (2015) suggested that the magnetic field lines threading the front edges of the patches must have evolved about 1.0–2.1 hr from their opening at the dayside magnetopause to their reclosure by magnetotail reconnection under a slow and thin solar wind condition (Vsw ≈ 380 km/s, Nsw ≈ 2 cm^{-3}).

4. Conclusion

In this work, we have presented simultaneous observations from multiple GPS TEC, SuperDARN, DMSP satellite, and the MHD simulation to show a "wave-like" evolution of patches modulated by magnetopause reconnection and magnetotail reconnection. The"wave-like"structure refers to how multiple patches are arranged from the dayside to the nightside, gradually lengthening along the zonal direction, and their boundary curvatures all point toward the same center. Those patches formed near the dynamic cusp and were transported across the polar cap toward the nightside auroral oval under the effect of the IMF-modulated ionospheric convection. As they moved to the nightside polar cap boundary, the extended magnetotail reconnection allowed them to exit the polar cap. Convection can further decompose them into smaller plasma blobs, which will enter the return flow at auroral latitudes. In this work, we have combined simulation and observation data to document the extended magnetic reconnection in the dusk magnetotail and also to illustrate the role of IMF and dayside reconnection on the "wave-like" evolution of patches.

Data Availability Statement

The solar wind and IMF data from the ACE spacecraft is available at the NASA CDAWeb site via https://cdaweb.gsfc.nasa.gov/sp_phys/data/ace/mag/level_2_cdaweb/mfi_h0/2014/ (NASA, 2024). The DMSP in-situ particle data and GPS TEC data used for observing the patch plasma parameters and motion are available at CEDAR Madrigal via http://cedar.openmadrigal.org/list/ (registering personal information and choosing "Defense meteorological satellite Program" or "World-wide GNSS Receiver Network") (CEDAR, 2024). The SuperDARN convection data used for obtaining the polar ionospheric convection patterns and the 3D PPMLR-MHD simulation data used for obtaining the 3D topology of magnetic field lines on 27 February 2014 are stored in https://doi.org/10.5281/zenodo.13353693 (Zhang et al., 2024).

Acknowledgments

This work is supported by the National Natural Science Foundation of China (Grants 42325404, 42120104003, 42204164, 42474219), the Chinese Meridian Project, the Shandong Provincial Natural Science Foundation (Grant ZR2022MD034), the International Partnership Program of Chinese Academy of Sciences (Grant 183311KYSB20200003), Xiaomi Young Talents Program, the foundation of the National Key Laboratory of Electromagnetic Environment (Grant JCKY2022210C614240301), National Program on Key Basic Research Project (2022-173-SD-1) and the International Collaboration Supporting Project. S.-R. Zhang receives partial support from NSF co-operative agreement ATM-0733510. The work in Norway is supported by the Research Council of Norway Grant 326039. Work at UCLA has been supported by NSF Grant AGS-2055192. This research was supported by the International Space Science Institute (ISSI) in Bern and Beijing, through ISSI International Team project #511 (Multi-Scale Magnetosphere-Ionosphere-Thermosphere Interaction). SuperDARN is a collection of radars funded by national scientific funding agencies of Australia, Canada, China, France, Japan, South Africa, United Kingdom, and United States of America.

References

Carlson, H. C., Oksavik, K., Moen, J., & Pedersen, T. (2004). Ionospheric patch formation: Direct measurements of the origin of a polar cap patch. *Geophysical Research Letters*, *31*(8), L08806. https://doi.org/10.1029/2003GL018166

CEDAR. (2024). The DMSP in-situ particle data and GPS TEC data [Dataset]. Retrieved from http://cedar.openmadrigal.org/list/

Chisham, G., Lester, M., Milan, S., Freeman, M., Bristow, W., Grocott, A., et al. (2007). A decade of the super dual auroral radar network (superdarn): Scientific achievements, new techniques and future directions. *Surveys in Geophysics*, *28*(1), 33–109. https://doi.org/10.1007/s10712-007-9017-8

Colella, P., & Woodward, P. R. (1984). The piecewise parabolic method (ppm) for gas-dynamical simulations. *Journal of Computational Physics*, *54*(1), 174–201. https://doi.org/10.1016/0021-9991(84)90143-8

Coster, A. J., Foster, J., & Erickson, P. (2003). Monitoring the ionosphere with GPS: Space weather. *GPS World*, *14*(5), 42.

Cowley, S. W. H. (1982). The causes of convection in the Earth's magnetosphere—A review of developments during the IMS. *Review of Geophysics*, *20*(3), 531–565. https://doi.org/10.1029/rg020i003p00531

Crowley, G. (1996). Critical review of ionospheric patches and blobs. In W. R. Stone (Ed.), *Review of radio science 1992–1996* (pp. 619–648). Oxford University Press.

Dungey, J. W. (1961). Interplanetary magnetic field and the auroral zones. *Physical Review Letters*, *6*(2), 47–48. https://doi.org/10.1103/physrevlett.6.47

Foster, J. C. (1993). Storm time plasma transport at middle and high latitudes. *Journal of Geophysical Research*, *98*(A2), 1675–1689. https://doi.org/10.1029/92JA02032

Foster, J. C., & Burke, W. J. (2002). Saps: A new categorization for sub-auroral electric fields. *Eos Transactions of AGU*, *83*(36), 393–394. https://doi.org/10.1029/2002EO000289

Foster, J. C., Coster, A. J., Erickson, P. J., Holt, J. M., Lind, F. D., Rideout, W., et al. (2005). Multiradar observations of the polar tongue of ionization. *Journal of Geophysical Research*, *110*(A9), A09S31. https://doi.org/10.1029/2004JA010928

Foster, J. C., Coster, A. J., Erickson, P. J., Rich, F. J., & Sandel, B. R. (2004). Stormtime observations of the flux of plasmaspheric ions to the dayside cusp/magnetopause. *Geophysical Research Letters*, *31*(8), L08809. https://doi.org/10.1029/2004GL020082

Foster, J. C., Zou, S., Heelis, R. A., & Erickson, P. J. (2021). Ionospheric storm enhanced density plumes. In C. S. Huang & G. Lu (Eds.), *Space physics and aeronomy collection volume 3: Ionosphere dynamics and applications, geophysical monograph 260* (1st ed., pp. 117–126). https://doi.org/10.1002/9781119815617.ch6

Genestreti, K. J. (2016). *Spatial characteristics of magnetotail reconnection (Order No. 10240757)*. ProQuest Dissertations & Theses Global. (1865331110).

Goldstein, J., & Sandel, B. R. (2005). The global pattern of evolution of plasmaspheric drainage plumes. In *Inner magnetosphere interactions: New perspectives from imaging* (pp. 1–22). American Geophysical Union (AGU). https://doi.org/10.1029/159GM02

Greenspan, M. E., Anderson, P. B., & Pelagatti, J. M. (1986). Characteristics of the thermal plasma monitor (SSIES) for the Defense meteorological satellite Program (DMSP) spacecraft S8 through F10. *Technical Report AFGL- TR-86- 0227. Hanscom AFB*.

Grocott, A., Milan, S. E., Yeoman, T. K., Sato, N., Yukimatu, A. S., & Wild, J. A. (2010). Superposed epoch analysis of the ionospheric convection evolution during substorms: IMF BY dependence. *Journal of Geophysical Research*, *115*(A5), A00I06. https://doi.org/10.1029/2010JA015728

Hairston, M. R., & Heelis, R. A. (1995). Response time of the polar ionospheric convection pattern to changes in the north-south direction of the IMF. *Geophysical Research Letters*, *22*(5), 631–634. https://doi.org/10.1029/94gl03385

Hardy, D. A., Holeman, E. G., Burke, W. J., Gentile, L. C., & Bounar, K. H. (2008). Probability distributions of electron precipitation at high magnetic latitudes. *Journal of Geophysical Research*, *113*(A6), A06305. https://doi.org/10.1029/2007JA012746

Hosokawa, K., Moen, J. I., Shiokawa, K., & Otsuka, Y. (2011). Decay of polar cap patch. *Journal of Geophysical Research*, *116*(5), A05306. https://doi.org/10.1029/2010JA016297

Hosokawa, K., Taguchi, S., & Ogawa, Y. (2016). Edge of polar cap patches. *Journal of Geophysical Research: Space Physics*, *121*(4), 3410–3420. https://doi.org/10.1002/2015JA021960

Hosokawa, K., Taguchi, S., Ogawa, Y., & Aoki, T. (2013). Periodicities of polar cap patches. *Journal of Geophysical Research: Space Physics*, *118*(1), 447–453. https://doi.org/10.1029/2012JA018165

Hu, Y., Guo, X., & Wang, C. (2007). On the ionospheric and reconnection potentials of the Earth: Results from global MHD simulations. *Journal of Geophysical Research*, *112*(A7), A07215. https://doi.org/10.1029/2006JA012145

Knudsen, W. C. (1974). Magnetospheric convection and the high-latitude F2 ionosphere. *Journal of Geophysical Research*, *79*(7), 1046–1055. https://doi.org/10.1029/ja079i007p01046

Koga, D., Gonzalez, W. D., Souza, V. M., Cardoso, F. R., Wang, C., & Liu, Z. K. (2019). Dayside magnetopause reconnection: Its dependence on solar wind and magnetosheath conditions. *Journal of Geophysical Research: Space Physics*, *124*(11), 8778–8787. https://doi.org/10.1029/2019ja026889

Lockwood, M., & Carlson, H. C. (1992). Production of polar cap electron density patches by transient magnetopause reconnection. *Geophysical Research Letters*, *19*(17), 1731–1734. https://doi.org/10.1029/92GL01993

Lockwood, M., Davies, J. A., Moen, J., Van Eyken, A. P., Oksavik, K., McCrea, I. W., & Lester, M. (2005). Motion of the dayside polar cap boundary during substorm cycles: II. Generation of poleward-moving events and polar cap patches by pulses in the magnetopause reconnection rate. *Annales Geophysicae*, *23*(11), 3513–3532. https://doi.org/10.5194/ANGEO-23-3513-2005

Lockwood, M., & Moen, J. (1999). Reconfiguration and closure of lobe flux by reconnection during northward IMF: Possible evidence for signatures in cusp/cleft auroral emissions. *Annales Geophysicae*, *17*(8), 996–1011. https://doi.org/10.1007/s00585-999-0996-2

Lorentzen, D. A., Moen, J., Oksavik, K., Sigernes, F., Saito, Y., & Johnsen, M. G. (2010). In situ measurement of a newly created polar cap patch. *Journal of Geophysical Research*, *115*(A12), A12323. https://doi.org/10.1029/2010JA015710

Lorentzen, D. A., Shumilov, N., & Moen, J. (2004). Drifting airglow patches in relation to tail reconnection. *Geophysical Research Letters*, *31*(2), L02806. https://doi.org/10.1029/2003GL017785

Ma, Y.-Z., Zhang, Q.-H., Xing, Z.-Y., Heelis, R. A., Oksavik, K., & Wang, Y. (2018). The ion/electron temperature characteristics of polar cap classical and hot patches and their influence on ion upflow. *Geophysical Research Letters*, *45*(6), 8072–8080. https://doi.org/10.1029/2018GL079099

Moen, J., Gulbrandsen, N., Lorentzen, D. A., & Carlson, H. C. (2007). On the MLT distribution of F region polar cap patches at night. *Geophysical Research Letters*, *34*(14), L14113. https://doi.org/10.1029/2007GL029632

Moen, J., Qiu, X. C., Carlson, H. C., Fujii, R., & McCrea, I. W. (2008). On the diurnal variability in F2-region plasma density above the EISCAT Svalbard radar. *Annales Geophysicae*, *26*(8), 2427–2433. https://doi.org/10.5194/angeo-26-2427-2008

Mori, D., & Koustov, A. V. (2013). SuperDARN cross polar cap potential dependence on the solar wind conditions and comparisons with models. *Advances in Space Research*, *52*(6), 1155–1167. https://doi.org/10.1016/j.asr.2013.06.019

Nagai, T., Shinohara, I., Saito, Y., Ieda, A., & Nakamura, R. (2023). Location and timing of magnetic reconnections in earth's magnetotail: Accomplishments of the 29-year geotail near-earth magnetotail survey. *Journal of Geophysical Research: Space Physics*, *128*(12), e2023JA032023. https://doi.org/10.1029/2023ja032023

NASA. (2024). Solar wind and IMF data from the ACE spacecraft [Dataset]. Retrieved from https://cdaweb.gsfc.nasa.gov/sp_phys/data/ace/mag/level_2_cdaweb/mfi_h0/2014/

Oksavik, K., Barth, V. L., Moen, J., & Lester, M. (2010). On the entry and transit of high-density plasma across the polar cap. *Journal of Geophysical Research*, *115*(A12), A12308. https://doi.org/10.1029/2010JA015817

Oksavik, K., Ruohoniemi, J. M., Greenwald, R. A., Baker, J. B. H., Moen, J., Carlson, H. C., et al. (2006). Observations of isolated polar cap patches by the European Incoherent Scatter (EISCAT) Svalbard and super dual auroral radar network (SuperDARN) Finland radars. *Journal of Geophysical Research*, *111*(A5), A05310. https://doi.org/10.1029/2005JA011400

Pettigrew, E. D., Shepherd, S. G., & Ruohoniemi, J. M. (2010). Climatological patterns of high-latitude convection in the Northern and Southern hemispheres: Dipole tilt dependencies and interhemispheric comparisons. *Journal of Geophysical Research*, *115*(A7), A07305. https://doi.org/10.1029/2009JA014956

Ruohoniemi, J., & Baker, K. (1998). Large-scale imaging of high-latitude convection with super dual auroral radar network HF radar observations. *Journal of Geophysical Research*, *103*(A9), 20797–20811. https://doi.org/10.1029/98ja01288

Ruohoniemi, J. M., Shepherd, S. G., & Greenwald, R. A. (2002). The response of the high-latitude ionosphere to IMF variations. *Journal of Atmospheric and Solar-Terrestrial Physics*, *64*(2), 159–171. https://doi.org/10.1016/s1364-6826(01)00081-5

Scurry, L., Russell, C. T., & Gosling, J. T. (1994). Geomagnetic activity and the beta dependence of the dayside reconnection rate. *Journal of Geophysical Research*, *99*(A8), 14811–14814. https://doi.org/10.1029/94JA00794

Siscoe, G. L. (1982). Energy coupling between regions 1 and 2 Birkeland current systems. *Journal of Geophysical Research*, *87*(A7), 5124–5130. https://doi.org/10.1029/JA087iA07p05124

Tang, B., & Wang, C. (2018). Large scale current systems developed from substorm onset: Global MHD results. *Science China Technological Sciences*, *61*(3), 389–396. https://doi.org/10.1007/s11431-017-9132-y

Tenfjord, P., Østgaard, N., Snekvik, K., Laundal, K. M., Reistad, J. P., Haaland, S., & Milan, S. E. (2015). How the IMF by induces a by component in the closed magnetosphere and how it leads to asymmetric currents and convection patterns in the two hemispheres. *Journal of Geophysical Research: Space Physics*, *120*(11), 9368–9384. https://doi.org/10.1002/2015JA021579

Thomas, E. G., Baker, J. B. H., Ruohoniemi, J. M., Clausen, L. B. N., Coster, A. J., Foster, J. C., & Erickson, P. J. (2013). Direct observations of the role of convection electric field in the formation of a polar tongue of ionization from storm enhanced density. *Journal of Geophysical Research: Space Physics*, *118*(3), 1180–1189. https://doi.org/10.1002/jgra.50116

Wood, A. G., Pryse, S. E., & Moen, J. (2009). Modulation of nightside polar patches by substorm activity. *Annales Geophysicae*, *27*(10), 3923–3932. https://doi.org/10.5194/angeo-27-3923-2009

Zhang, D., Zhang, Q., Oksavik, K., Tang, B.-B., Zhang, Y.-L., Lockwood, M., et al. (2024). SuperDARN convection data and the 3D PPMLR-MHD simulation data on 27 February 2014 [Dataset]. *Zenodo*. https://doi.org/10.5281/zenodo.13353693

Zhang, Q.-H., Lockwood, M., Foster, J. C., Zhang, S.-R., Zhang, B.-C., McCrea, I. W., et al. (2015). Direct observations of the full Dungey convection cycle in the polar ionosphere for southward interplanetary magnetic field conditions. *Journal of Geophysical Research*, *120*(6), 4519–4530. https://doi.org/10.1002/2015JA021172

Zhang, Q.-H., Moen, J. I., Lockwood, M., McCrea, I., Zhang, B.-C., McWilliams, K. A., et al. (2016). Polar cap patch transportation beyond the classic scenario. *Journal of Geophysical Research: Space Physics*, *121*(9), 9063–9074. https://doi.org/10.1002/2016JA022443

Zhang, Q.-H., Xing, Z.-Y., Wang, Y., & Ma, Y.-Z. (2020). Formation and evolution of polar cap ionospheric patches and their associated upflows and scintillations: A review. In Q. G. Zong, P. Escoubet, D. Sibeck, G. Le, & H. Zhang (Eds.), *Dayside magnetosphere interaction* (pp. 286–302). John Wiley & Sons, Inc. https://doi.org/10.1002/9781119509592.ch16

Zhang, Q.-H., Zhang, B.-C., Hu, H.-Q., Moen, J., Lockwood, M., McCrea, I. W., et al. (2013). Polar cap patch segmentation of the tongue of ionization in the morning convection cell. *Geophysical Research Letters*, *40*(12), 2918–2922. https://doi.org/10.1002/grl.50616

Zhang, Q.-H., Zhang, B.-C., Lockwood, M., Hu, H.-Q., Moen, J. I., Ruohoniemi, J. M., et al. (2013). Direct observations of the evolution of polar cap ionization patches. *Science*, *339*(6127), 1597–1600. https://doi.org/10.1126/science.1231487

Zhang, Y., Paxton, L. J., & Lui, A. T. Y. (2007). Polar rain aurora. *Geophysical Research Letters*, *34*(20), L20114. https://doi.org/10.1029/2007gl031602